Marine Geology 495 (2026) 107749

Contents lists available at ScienceDirect

Marine Geology

journal homepage: www.elsevier.com/locate/margo

Research Article

Luminescence as a tool to reconstruct sediment transport pathways in a tidal inlet

Anna Maartje de Boer [a,*], Stuart Pearson [b], Ad van der Spek [c,d], Bram van Prooijen [b], Jakob Wallinga [a]

[a] Soil Geography and Landscape Group & Netherlands Centre for Luminescence Dating, Wageningen University & Research, Droevendaalsesteeg 3, 6708 PB Wageningen, the Netherlands
[b] Faculty of Civil Engineering & Geosciences, Delft University of Technology, Stevinweg 1, 2628 CN Delft, the Netherlands
[c] Geological Survey of the Netherlands, 3508 TA Utrecht, the Netherlands
[d] Deltares, 2600 MH Delft, the Netherlands

ARTICLE INFO

Editor: N Senechal

Keywords:
Single-grain luminescence
Feldspar IRSL
Differential bleaching
Sediment pathways
Tidal inlet
Coastal nourishment

ABSTRACT

Luminescence dating methods are widely used to date coastal sediments, while luminescence tracing methods are a novel application to reconstruct coastal sediment pathways. Both methods rely on subaqueous resetting (bleaching) of luminescence signals by light. Differences in bleaching between grains and/or luminescence signals encode information on the light exposure history of individual grains and therefore yield information on past sediment transport. Here we assess the potential of multi-signal single-grain feldspar luminescence to inform about sediment pathways at Ameland tidal inlet in the Dutch Wadden Sea. We also tested whether nourished and native sands can be distinguished based on their luminescence signals.

Single-grain infrared stimulated luminescence (IRSL50) and post-IR IRSL (pIRIR) were measured from samples collected from modern sea-floor deposits across the inlet. Equivalent dose (D_e) distributions were assessed using the Central Age Model (CAM), and bootstrapped versions of the Minimum Age Model (bMAM) and Maximum Age Model (bMAX) were applied to the IRSL50 D_e distributions. Spatial trends in CAM and bMAX-De reveal highest inherited doses at the tip of Ameland in the Borndiep channel, decreasing along transport pathways around the ebb-tidal delta. These patterns indicate erosion of Pleistocene sediments in the Borndiep channel and progressive bleaching of luminescence signals upon transport. Low D_e values in shallow areas reflect repeated reworking of Holocene sands within the active layer. Nourished and native sediments show indistinguishable luminescence characteristics for our dataset due to their shared Holocene origin.

1. Introduction

Coastal nourishments are widely implemented in the Dutch coastal zone to sustain sediment budgets and mitigate erosion (Brand et al., 2025; Brand et al., 2022). Their effectiveness depends not only on the total sand volume, but also on the pathways along which (nourished) sand is redistributed. The better we understand sediment pathways, the better we can optimize the nourishment location. In tidal inlets and estuaries, sediment pathways are particularly complex (Pearson, 2022). Tides, waves and storms (re)shape the inlet constantly and causes channels to migrate and sediment to exchange with adjacent coasts and tidal basins. Quantifying sediment pathways remains a challenge, as traditional monitoring approaches like bathymetric surveys, remote sensing, and hydrodynamic modelling provide only local information or system-scale patterns (Elias et al., 2022; Elias et al., 2012; van der Spek, 2018; Wang et al., 2018). There is a clear need for field methods to identify sediment pathways which can validate model predictions of grain transport (e.g., Pannozzo et al., 2025; van Westen et al., 2025).

Several sediment tracing techniques exist, yet each has clear drawbacks in this context. Artificial tracers such as fluorescent (Gallaway et al., 2012; Kraus et al., 1982; Miller and Komar, 1979; Murray, 1967; Oliveira et al., 2017; Pearson et al., 2021a) or magnetic (Black et al., 2007; Romão et al., 2024) coatings are recoverable but alter grain properties and are logistically demanding at the scales of tidal inlets. Radioisotopes and natural radionuclides are unsuitable for medium- to coarse-grained sands and raise safety concerns (Crickmore and Lean,

* Corresponding author.
E-mail address: anna-maartje.deboer@wur.nl (A.M. de Boer).

https://doi.org/10.1016/j.margeo.2026.107749
Received 30 October 2025; Received in revised form 22 January 2026; Accepted 11 March 2026
Available online 12 March 2026

1962; Eisma et al., 1989; Giffin and Corbett, 2003). Geochemical and magnetic susceptibility methods (Clemens and Komar, 1988; Gallaway et al., 2012) likely cannot reliably distinguish nourished from native sand in the Dutch coastal system as properties of Dutch coastal sand are too similar. These limitations highlight the need for an intrinsic tracer that can distinguish nourished and native sand grains without modifying them.

Luminescence offers such potential. Mineral grains store charge in crystal defects when exposed to ionizing environmental radiation, and empty upon sunlight exposure or heat (Huntley et al., 1985; Rhodes, 2011). Incomplete resetting, i.e., poor bleaching, of this build-up dose may lead to a remnant dose upon deposition. For luminescence dating, signals need to be reset in all grains or well-bleached grains need to be identified by measuring small aliquot or single-grains and appropriate statistical approaches (e.g. Brill et al., 2018; Mauz et al., 2010). While poor bleaching is a challenge for dating, it may be an asset when luminescence signals are used for inferring information on light exposure duration and/or mixing of grains with different light exposure histories. There are three ways to study bleaching: (i) identify the scatter in equivalent dose (D_e) distributions, preferable at the single-grain level; (ii) compare signals of different bleachability at sample level (e.g. Reimann et al., 2015); (iii) compare signals of different bleachability at the grain level (e.g. Choi et al., 2024). Luminescence signals from feldspar are particularly well suited for studying bleaching patterns, as signals of different bleachability can be measured on a single grain: Infrared stimulated luminescence (IRSL) measured at low-temperatures (~50 °C) bleaches rapidly, whilst several post-IR IRSL signals measured at higher temperatures bleach slower (Cheng et al., 2022; de Boer et al., 2024b; Thomsen et al., 2008). A detailed explanation on all luminescence acronyms in this work can be found in the Luminescence Glossary in Supplement S1.

The Ameland inlet provides a unique case study for studying sediment pathways and the dispersal of nourishment sand. In 2018, approximately 5 million m^3 of sand was placed as the first ebb-tidal delta nourishment in the Netherlands, with the dual aim of reinforcing the Ameland coast and testing whether such interventions can feed sediment budgets of the wider Wadden Sea. Extensive monitoring programs (e.g., KUSTGENESE 2.0, SEAWAD) have quantified large-scale morphological and ecological responses, but detailed redistribution of nourishment sand at the grain scale remains poorly understood (Pearson et al., 2021a; Pearson et al., 2020; Van Prooijen et al., 2020). Recently developed particle-tracking models now allow simulation of possible transport scenarios but still require validation with field-based tracers (Pearson, 2022; Romão et al., 2024; van Westen et al., 2025).

Recent studies have demonstrated the ability of luminescence to reveal pathways of sediment transport in fluvial (Guyez et al., 2022; Guyez et al., 2023; Rhodes and Leathard, 2022) and coastal (Ahmed et al., 2014; Gray et al., 2019; Reimann et al., 2015) environments. In this study, we evaluate the potential of multi-signal single-grain feldspar luminescence to (i) assess whether luminescence signals give insight into sediment transport pathways across the Ameland tidal inlet, (ii) test whether nourished and native sediments can be distinguished based on their luminescence properties, and (iii) identify key steps for future development of luminescence as a sediment tracing method.

2. Study area: Ameland Tidal inlet

2.1. Morphodynamics

Our study area is located in and around the Ameland Inlet in the Dutch Wadden Sea (Fig. 1). It is bounded by the barrier islands of Terschelling in the west and Ameland in the east. The inlet connects the Wadden sea basin to its south with the North sea. The ebb-tidal delta is situated on the North Sea side of the inlet. The Borndiep channel is the main channel in the inlet and separates the Boschplaat from Ameland. The Ameland Inlet is highly dynamic and shaped by the competition

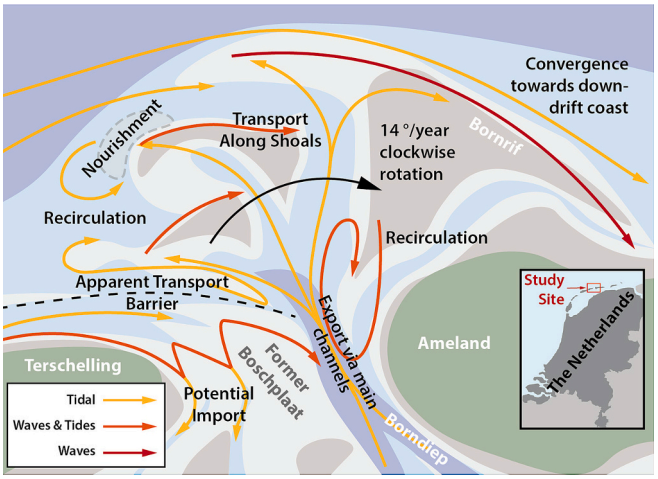

Fig. 1. Overview of main sediment pathways on Ameland ebb-tidal delta after Pearson (2022). The pathways are a combination of tides and waves (colors). Clockwise rotation dominates main transport routes. The nourishment is shown in light gray.

between strong tidal currents and wave action. The tide is semidiurnal and mesotidal (spring tidal range of 2.5 m) with a strong flood-dominant tidal asymmetry offshore of the inlet. The outer delta is subject to an average annual significant wave height of 1.37 m, with waves primarily from the northwest (Elias et al., 2019). Direct freshwater inflow is limited, although winds from the southwest tend to transport water from sluices, leading to weak periodic stratification (Duran-Matute et al., 2014). Field observations and modelling indicate that wind-driven transport across tidal watersheds during storms and other strong wind events leads to a substantial net outflow through the Ameland Inlet (Donatelli et al., 2022; van Weerdenburg et al., 2021).

The Boschplaat is incised and continually reworked by several highly mobile channels. The ebb-tidal delta is characterized by clockwise-migrating channels and shoals. This rotation occurs at an average of 14°/year and leads to extensive reworking of surface deposits. The western half of the delta is excavated deeply by larger ebb channels while the eastern half (the Bornrif platform) is much more stable (Pearson et al., 2022) (Fig. 1).

The ebb-tidal delta predominantly consists of fine sand (d_{50} mostly between 170 and 230 μm), and exhibits a tendency to fine in a clockwise direction around the inlet (Elias et al., 2022). The coarsest sediment (d_{50} > 300 μm) can be found in the deeper channels. Fine sediment is regularly ejected from the Wadden Sea on the ebb tide and remains in suspension over the outer delta (Pearson et al., 2021b), although conditions are generally too energetic for it to settle there.

Alongshore transport estimates in the literature vary widely, but suggest an annual eastward transport along the Terschelling coast of 0.3–1.0 × 10^6 m^3 (Elias et al., 2019). From the Terschelling coast and shoreface, sediment follows two main pathways: (1) it is transported into the Wadden Sea where it is deposited (Elias et al., 2012) or ejected out the main ebb-channel (Borndiep), or (2) it bypasses the inlet, driven by the strong flood-tidal asymmetry and wave-driven currents around or onto the ebb-tidal delta. Sediment on the delta then generally migrates clockwise around the inlet, eventually reaching the Ameland coast (Pearson et al., 2022). An estimated 0.8–1.2 × 10^6 m^3 of sediment then follows the Ameland coast (Ridderinkhof et al., 2016) and continues eastward. Loss of sediment from the system is replenished by frequent shoreface and beach nourishments around the tidal inlet of Ameland (Brand et al., 2022), the borrow areas of these nourishments are situated in the North Sea and source deposits are all of Holocene origin.

The long-term sediment sink in this system are the tidal flats of the Wadden Sea. Sand that is not retained within the basin is transported back offshore and deposited on the ebb-tidal delta. From there, sediment

is redistributed alongshore toward the downdrift barrier island and enters the next inlet where the cycle repeats. The ebb-tidal delta can be considered a short-term sediment sink, whereas the Wadden Sea tidal flats represent a long-term sink (Elias et al., 2012).

2.2. Geology

In the subsurface of the Ameland inlet and vicinity, deposits from the Elsterian (MIS 12 or 10), Saalian (MIS 6) and Weichselian (MIS 5d-2) glaciations occur (Fig. 2). At the eastern part of Terschelling Holocene tidal channel deposits overly Saalian glacial tills (Drenthe Formation – Gieten Member), middle Pleistocene sands (Urk Formation) and coastal deposits from the Eemian interglacial (Peelo Formation) (Fig. 2). Underneath western Ameland, compact Elsterian pot clay occurs at depths of 25 to 30 m, and is locally exposed in the Borndiep inlet channel. The very compact Elsterian pot clay and the boulder- and gravel rich Saalian glacial till are typical erosion-resistant deposits that potentially affect the local morphodynamics (Pierik et al., 2023). Weichselian eolian cover sands are the youngest Pleistocene deposit, occuring where the top of the Pleistocene is not eroded by migrating tidal channels in the Holocene. The glacial deposits alternate with coastal and estuarine deposits that were formed during the Holsteinian (MIS 11), Eemian (MIS 5e) and Holocene (MIS 1) interglacials. These deposits consist of tidal channel sands and finer-grained sediments deposited in an estuarine setting. Lateral transition into organic-rich deposits occurs. These coastal deposits originating from different interglacials are similar and occasionally cut into each other. They are therefore difficult to distinguish unless separated by glacial sediments.

The Holocene tidal channel deposits can consist of several generations of channels, each of them characterized by a coarse-grained, shell-rich channel lag. The continuous migration and local increase of channel dimensions results in progressively deeper reworking and erosion and, in cases, incising into underlying deposits, exposing Holocene and Pleistocene strata. The Borndiep channelcuts into Pleistocene deposits of the Urk Formation (NUUR1) and erodes the western Ameland shoreface (Fig. 2), thereby reworking older Holocene tidal and lagoonal deposits from the Naaldwijk Formation (NUNA). Smaller channels like the Boschgat do not reach the Pleistocene deposits but laterally rework Holocene deposits like the Zandvoort member (NUNAZA1). Bear in mind that the GeoTOP model is based on interpolations between a limited number of cores, therefore it is highly likely the Borndiep does erode into NUUR1 deposits, contrary to what the GeoTOP model shows here.

The Ameland inlet system is generally quartz dominated, with feldspar forming a subordinate but widespread component of the sediment. Previous studies from the Wadden Sea report quartz contents of ~80–85% in sand-sized fractions, while feldspar typically comprises ~7–16%, depending on grain size (Straaten, 1954; Van Straaten, 1964; Veenstra and Winkelmolen, 1976). Although mineralogical proportions vary with grain size, K-feldspar grains are expected to be well mixed

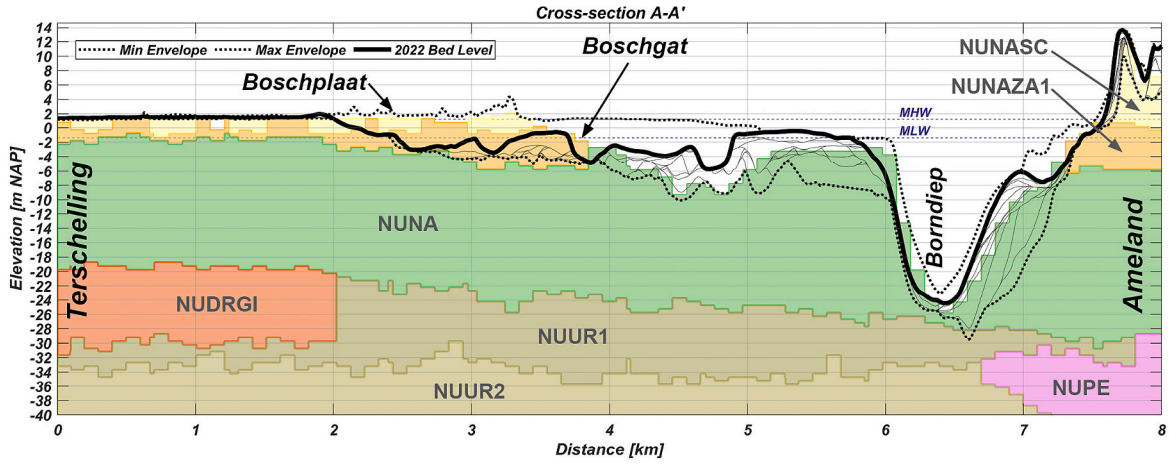

Code	Formation	Age	Lithology	Facies	Lithology: Details
NUNASC	Schoorl member	Holocene	sand	coastal dune	(v)f sand; local shells; peat layers / soils
NUNAZA1	Zandvoort member	Holocene	sand	shoreface, beach	f-m shelly sand
NUNA	Naaldwijk Fm.	Holocene	sand; clay	tidal channel, flat	f-m sand, marine shells; (silty) clay, shell layers, locally organic
NUDRGI	Drente Fm./ Gieten member	Saalian	diamict	basal till	very sandy to very silty clay and loam with gravel and boulders
NUUR1	Urk Fm .	middle Pleist.	sand	fluvial (Rhine)	f-vc, slightly to very gravelly sand
NUPE	Peelo Fm.	Elsterian	sand; pot clay	sub-glacial valley; ice-marginal lake	vf-vc micaceous sand; lacustrine clay
NUUR2	Urk Fm .	middle Pleist.	sand	fluvial (Rhine)	f-vc, slightly to very gravelly sand

Fig. 2. Stratigraphic cross-section along transect A-A' (Fig. 3), overlaying the bathymetry-derived stratigraphy from Fig. 5 in Pearson et al. (2022) on stratigraphic units from the BRO GeoTOP v1.6.1 model (TNO-GDN, 2025), described in the table below. Thick dashed lines indicate the envelope of bathymetric change from 1975 to 2022, with a thick black line marking the 2022 surface. Mean Low Water (MLW, −1.4 m NAP) and Mean High Water (MHW, +1.2 m NAP) are indicated with light dashed lines. All units are part of the Upper Nort Sea group (NU). Note that members are sub-units of formations. The Schoorl and Zandvoort members are part of the Holocene Naaldwijk Formation (NUNA). The fluvial deposits of the Urk Formation are subdivided in different phases. Grainsize indications: vf-very fine; f-fine; m-medium; vc-very coarse.

with the bulk sand population. Consequently, the single-grain feldspar signals analyzed here are considered representative of the active sediment layer.

Recent vibrocores show that peat and clay layers occur at 11 m - NAP in the shoreface of western Ameland (not in cross-section) (Vermaas, 2018). These layers influence the erosive morphology of the eastern wall of Borndiep channel by forming a plateau (Forzoni et al., *2018*; Vermaas, 2018). A similar plateau at the same depth to the west of Borndiep suggests the occurrence of a clay layer here too (van Onselen, 2020). The reduced thickness of the Holocene channel deposits under central and east Ameland (not in cross-section) indicates that channel erosion has been less severe. Here, older Holocene fine-grained lagoonal deposits and basal peat layers can occur locally. The latter can be present at the shoreface of the island as well (van Heteren and van der Spek, 2003). The ebb-tidal delta consists predominantly of the deposits of migrating tidal channels (van der Spek et al., 2022). The oldest sediments in the inlet and ebb-tidal delta are exposed at the margins of deeper channels (envelope of bathymetric change in Fig. 2), while the majority of surface sediments have been deposited in the last 5 years (Pearson et al., 2022).

3. Materials and methods

3.1. Sample collection and preparation

Sediment samples were collected from the seafloor during research cruises over several years by boxcoring. Luminescence samples were extracted from the box-cores by horizontally inserting PVC tubes into the undisturbed sediment at about 10 cm below the surface. Fig. 3 shows the bathymetry and sampling locations for each campaign year. A full overview of samples and sample locations is provided in Supplement S3.

All samples were prepared at the Netherlands Centre for Luminescence dating (NCL) under amber light conditions. Sediment that was not light-exposed during sampling was taken from the inner portion of each tube, wet sieved to 212–250 μm, and treated with 10% HCl to remove

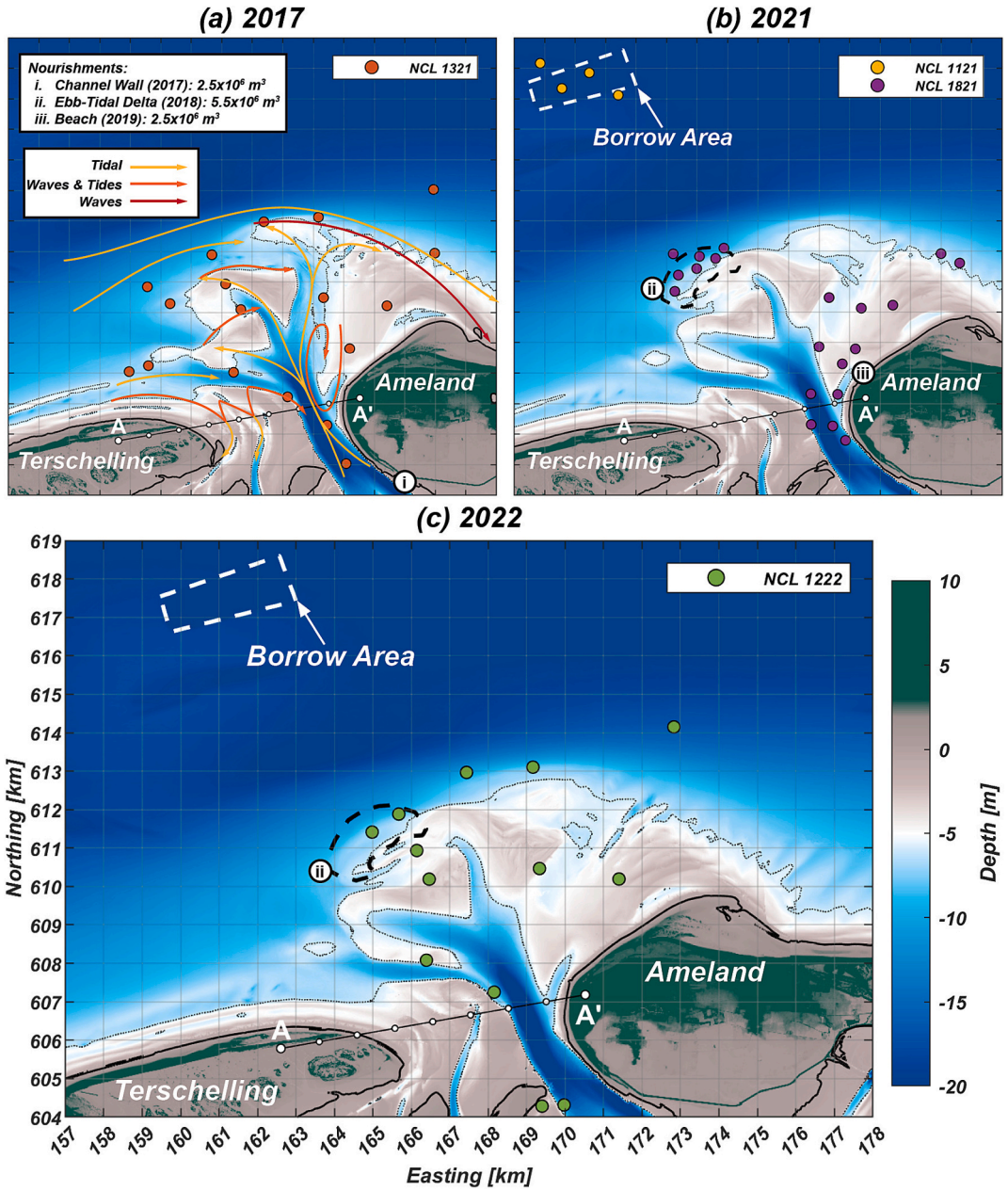

Fig. 3. Bathymetric maps with sample locations and nourishments from each sampling year. Transect A-A' corresponds to the location of the cross-section in Fig. 2. Sediment pathways in (a) correspond to those identified in Fig. 1.

carbonates and subsequently with 10% H_2O_2 to remove organic matter. A K-feldspar-rich fraction was isolated by density separation using LST fastfloat© with a density of 2.58 g/cm^3. We selected this grain size because it matches the d50 of the sand in the tidal inlet of Ameland (Elias et al., 2022; Van Prooijen et al., 2020) and is the standard fraction used for single-grain luminescence measurements (de Boer et al., 2024a).

3.2. Luminescence measurements

Single-grain analysis were performed using an EMCCD-based luminescence imaging system mounted on a Risø TL/OSL DA-20 reader, allowing direct measurement of infrared stimulated luminescence (IRSL) per grain (de Boer et al., 2024a; Kook et al., 2015). Luminescence signals were measured using the standard principles from the single aliquot regeneration (SAR) protocol for a multiple elevated temperature post-IR IRSL (MET-pIRIR) protocol at 50, 110, 170, and 230 °C (Supplement S4).

Emission was detected using a BG-3 + BG-39 (3.0 + 4.0 mm) blue filter package centered on 410 nm. Each measurement comprised 270 channels over 108 s (0.4 s per channel), with optical stimulation beginning at channel 11. Signal integration was carried out over the first 8 s of stimulation (channels 11–31), and background subtraction over the final 20 s of stimulation (channels 210–260).

Data were integrated over a 600 μm region of interest (ROI) using Risø Viewer+ software, a size shown to optimize signal detection while minimizing optical crosstalk. Dose-response curves were fitted using single saturating exponential functions, forced through the origin. Rejection thresholds for recycling ratio, recuperation relative to R1, and test dose uncertainty were set at 20%.

All analyses were conducted using the Luminescence package in R (Kreutzer and Developers, 2025). Equivalent doses were obtained using the CAM, bMAM, and bMAX models (see Section 3.3). A SAR-SARA test (Kars et al., 2014) was performed on one sample for each source type: pre-nourishment (NCL-1321), post-nourishment (NCL-1821) and nourishment borrow area (NCL-1121), to assess potential uncorrected sensitivity changes during the first SAR cycle for the MET-pIRIR protocol (Figs. 1–3 in Supplement S2).

3.3. Equivalent dose models

After feldspar signal measurement and equivalent dose (D_e) calculation for individual grains, three types of commonly used equivalent dose models were applied to obtain information from the D_e distribution. We construct abanico plots with the R package Luminescence (Kreutzer and Developers, 2025) to show a samples' equivalent dose distribution, dose frequency distribution, and the three model results. The plots also shows the standard error of each single-grain measurement in the D_e distributions. Abanico plots are an effective way to visualize luminescence data, however, they can be difficult to comprehend for non-specialists; a detailed explanation can be found in (Dietze et al., 2016).

To characterize bleaching behavior in our samples, we applied three equivalent dose models:

1. The **Central Age Model (CAM)** represents the mean dose and associated uncertainty, and also quantifies the overdispersion. Overdispersion is a measure of the spread within an equivalent dose distribution that cannot be explained by individual uncertainties of the single-grain equivalent dose estimates such as measurement uncertainty or parameter fitting (Galbraith et al., 1999). High CAM overdispersion (σ_{OD}) is often interpreted as indicative of heterogeneous bleaching, potentially caused by subaqueous sediment transport under turbid conditions (Brill et al., 2018; Cunningham et al., 2015). Values above 10% for small aliquot quartz (Rhodes, 2011) and above 25% for single-grain feldspar (Brill et al., 2018) are often considered to be indicative of heterogeneous bleaching. Overdispersion therefore serves as a valuable proxy for the degree of bleaching in a sample (Duller, 2008; Olley et al., 2004).
2. The **Minimum Age Model (MAM)** estimates the dose of the most-bleached grains in heterogeneously bleached samples (Galbraith et al., 1999) and is typically applied to heterogeneously bleached (fluvial) samples (Cunningham and Wallinga, 2012; Rodnight et al., 2006). We used the bootstrapped version of the MAM (bMAM) (Cunningham and Wallinga, 2012). Proper selection of the input sigma-b (σ_b) value is critical. This σ_b is the overdispersion expected for a well-bleached sample. Overestimation of σ_b will result in underestimating the burial dose when using the bMAM- D_e. We used a σ_b of 0.25 ± 0.05 based on (Brill et al., 2018). From this model we derived the statistic $p0_{MAM}$ and use it as a bleaching indicator. $p0_{MAM}$ denotes the proportion of grains attributed to the minimum dose component (Cunningham et al., 2015; Galbraith et al., 1999).
3. The **Maximum Age Model (MAX)** is derived from the MAM (Galbraith et al., 1999) but targets the oldest population in a sample (e.g. Deeben et al., 2010). We applied the bootstrapped MAX (bMAX), which similarly provides the $p0_{MAX}$ statistic, but here representing the proportion of grains attributed to the maximum dose.

4. Results

4.1. Test of measurement protocol

Before evaluating the single-grain equivalent dose data, we first verified that the measurement protocol performed reliably across all sample types using a SAR-SARA test for the MET-pIRIR protocol. The results (Fig. 1–3 in Supplement S2), show good agreement between measured and expected dose responses, with R^2 values for all fitted trendlines close to 1 and slopes within 10% of unity, confirming that the SAR procedure deals adequately with sensitivity change during measurement and provides robust estimates of absorbed dose across signals and dose levels.

4.2. Single-grain equivalent dose distributions

The single-grain abanico plots for the IRSL50 signal for four representative samples, one from each NCL project (Fig. 3), show broad distributions of equivalent doses (=absorbed dose) expressed in Gray (Gy, 1 Gy = J/kg) across the Ameland tidal inlet (Fig. 4 a-d). Each plot also includes model results for the bMAM, CAM, and bMAX D_e models which are discussed in section 4.3–4.5, as well as a small inset map with the sample location. Each black dot represents the equivalent dose from one sand grain. The majority of the dots are plotted on the left-side of the abanico plot, which means that their relative standard error is high and the precision is low. In terms of equivalent dose the distributions exhibit a broad scatter without clear populations of grains with similar dose. This wide spread in D_e values for the IRSL50 signal demonstrates substantial variability in the absorbed dose among individual grains. Abanico plots for the other feldspar signals (pIRIR110, pIRIR170, pIRIR230) are provided in Supplement S6 Fig. 5–62. The complete set of IRSL50 abanico plots for all samples (n = 58) can also be found in Supplement S6.

The number of accepted grains varies between samples and between signals (Fig. 5 and Supplement S3), but no clear spatial trends are observed (Fig. 4 in Supplement S5). Therefore we focus on D_e distributions rather than luminescence sensitivity to infer sediment pathways. To ensure robustness of the data used we rejected samples for which fewer than 15 grains were accepted for the IRSL50 signal for further analysis. Moreover, we restrict advanced age modelling (using bMAM and bMAX) to the IRSL50 data, and we do not attempt to compare De results obtained on individual grains using different signals.

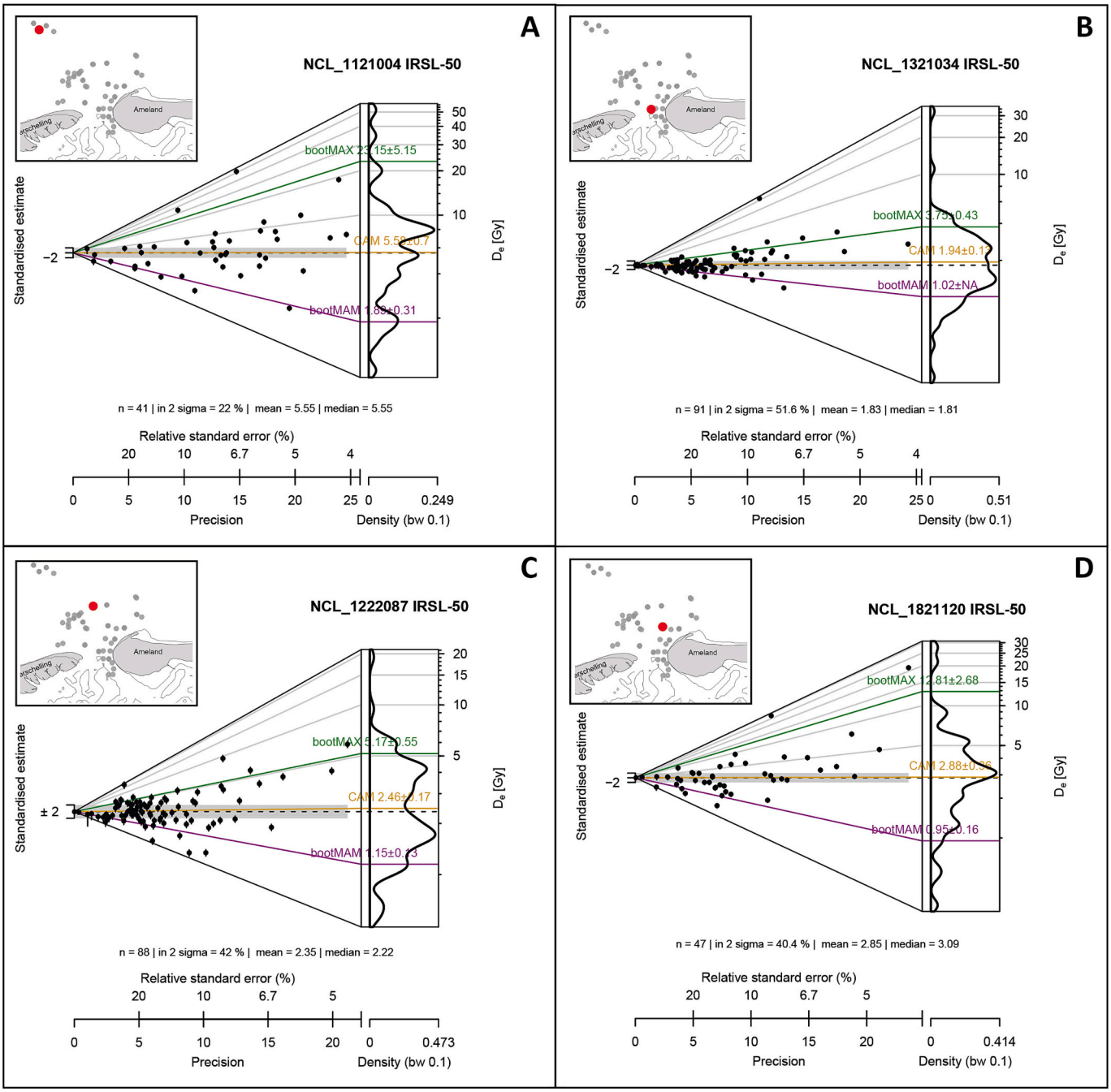

Fig. 4. Abanico plots of single-grain IRSL50 equivalent dose distributions for four representative samples from the tidal inlet of Ameland: A. NCL-1121004, B. NCL-1321034, C. NCL-1222087, and D. NCL-1821120. Each plot includes bMAM, CAM, and bMAX equivalent dose models and additional generic statistics as well as inset maps indicating the sample locations. IRSL50 abanico plots for all samples, as well as additional plots for pIRIR110, pIRIR170, and pIRIR230 signals, are provided in Supplement S6 Figs. 5–62.

4.3. Central age model and bleachability of feldspar signals

For all samples, inherited doses tend to increase systematically with read-out temperature of the luminescence signal. IRSL50 (Fig. 5a) shows the lowest CAM- D_e values, followed by pIRIR110 (Fig. 5b), pIRIR170 (Fig. 5c), and pIRIR230 (Fig. 5d). The plotted data represent CAM equivalent doses, reflecting the mean dose of the single-grain distributions. Across all signals, the highest CAM values occur at the northwestern tip of Ameland and in the channel bed deposits of the Borndiep. Even for IRSL50, these areas yield slightly elevated CAM values in comparison to other sample locations spread over the ebb-tidal delta. Samples from the nourishment borrow area (four points furthest north) show equal to slightly lower CAM values than samples from the Borndiep. Samples collected further offshore on the eastern ebb-tidal delta (Bornrif) also yield lower inherited doses than those of the Borndiep. The magnitude of the CAM doses is different for each feldspar signal, but the observed spatial patterns are similar across all feldspar signals of different bleachability.

4.4. Central age model and overdispersion

Fig. 6 shows IRSL50 CAM equivalent doses for all samples with at least 15 grains accepted sized to their associated overdispersion (OD). Uncertainties in both D_e and OD are provided in Supplement S3. The

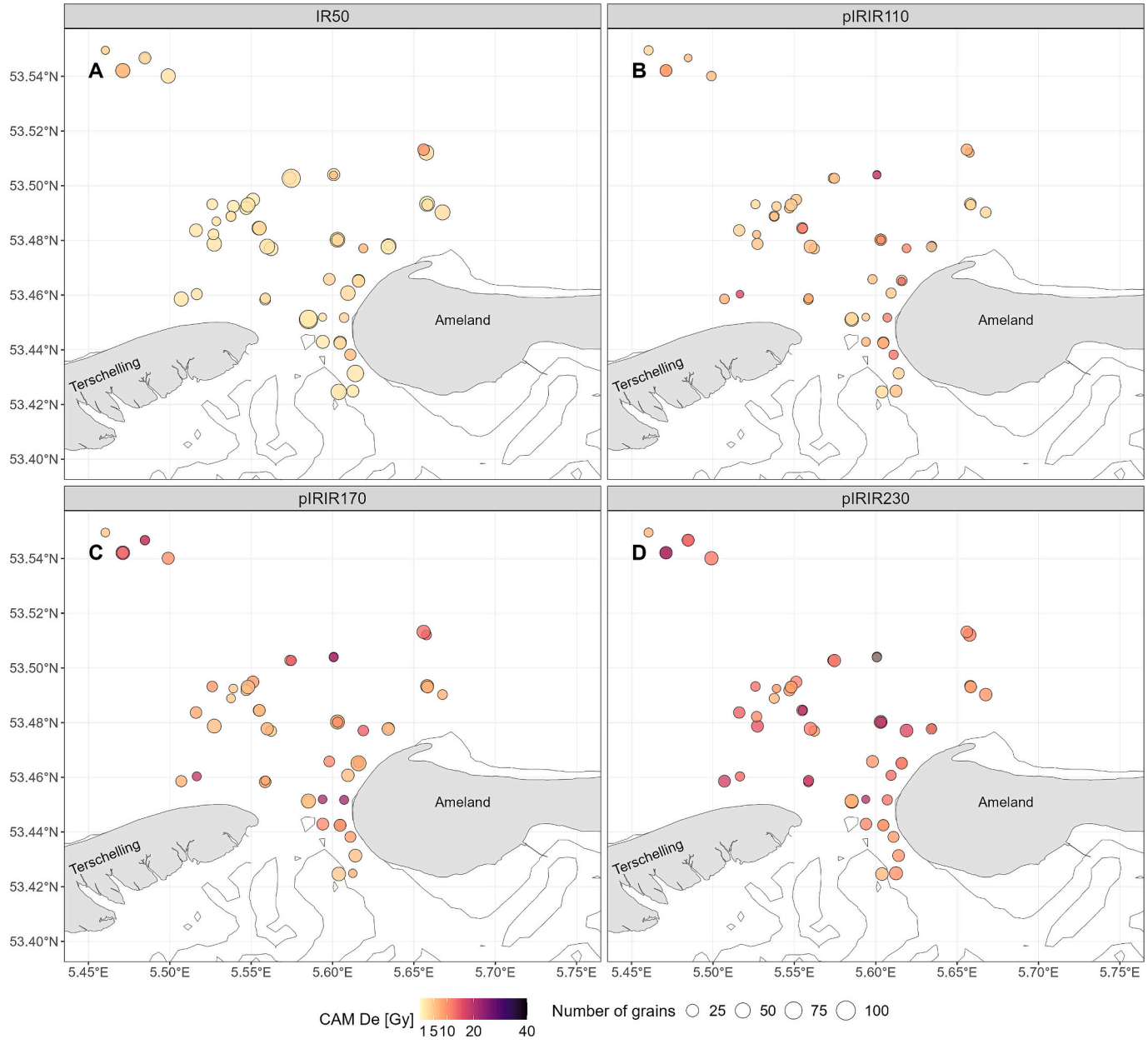

Fig. 5. Central Age Model equivalent doses for a. IRSL50, b. pIRIR110, c. pIRIR170, and d. pIRIR230 signals. Dot size represents the number of grains included in the calculation, while dot color indicates the corresponding CAM-De value.

lowest OD values, i.e. the smallest dots, occur at the nourishment borrow area. Samples near the tip of northwestern tip of Ameland in the Borndiep channel display the highest OD values. CAM D_e values are highest at the nourishment borrow area, at the northwestern tip in the Borndiep, and increase again toward the North Sea on the Bornrif platform.

4.5. Minimum and maximum age model and their bleaching metrics

Fig. 7a shows the bMAM equivalent doses across the tidal inlet of Ameland for the IR50 signal. Most values are very low (0–4 Gy), with slightly higher doses in offshore direction. At the nourishment borrow area, most samples fall within the low-dose range with one outlier. Further northeast in the direction of the North Sea on the Bornrif platform, bMAM D_e values reach up to 7.5 Gy. Dot size represents $p0_{MAM}$, the proportion of grains included in the minimum dose calculation. Larger dot sizes generally coincide with higher bMAM D_e values. The probability distribution of $p0_{MAM}$ (Fig. 7c) is skewed toward low values, with only a few offshore samples yielding higher contributions of grains to the minimum-age population.

Fig. 7b shows the bMAX equivalent doses, which range from 50 to 100 Gy at the northwestern tip of Ameland in the Borndiep and are lower everywhere else in the study area. Samples from the ebb tidal delta yield substantially lower bMAX D_e values, suggesting a reduced contribution of high-dose grains. At the nourishment borrow and placement sites, bMAX D_e values are similar. Dot size represents $p0_{MAX}$, the proportion of grains included in the maximum dose calculation. Spatial variation in $p0_{MAX}$ is limited, with only a few samples from the nourishment borrow

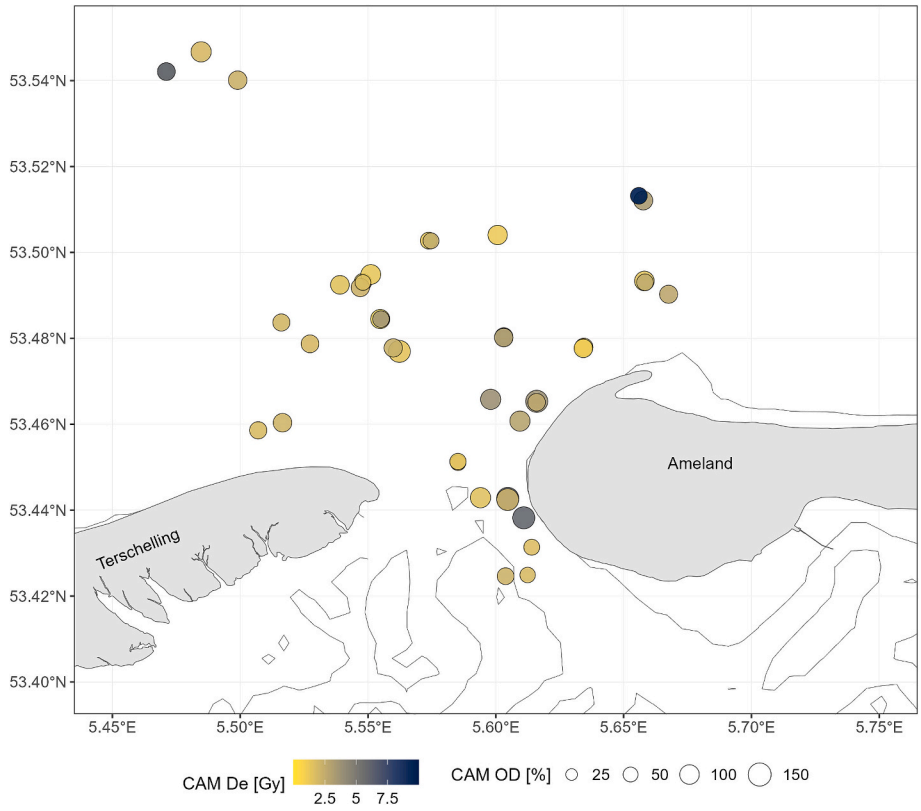

Fig. 6. Central Age Model (CAM) equivalent doses for the IRSL50 signal of samples collected in the Ameland tidal inlet. Dot color indicates CAM De in Gray and dot size represents overdispersion in percentage.

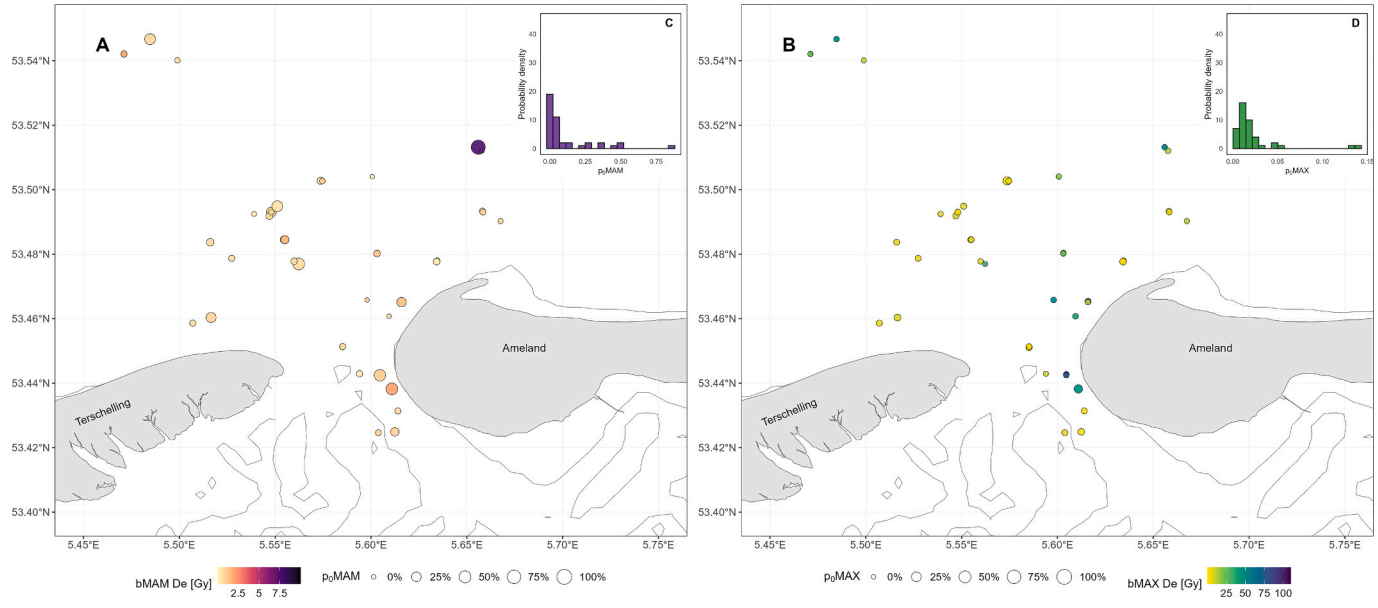

Fig. 7. a. Spatial distribution of bMAM equivalent doses (D_e) values for the IR50 signal, with dot size representing $p0_{MAM}$. b. Spatial distribution of bMAX equivalent doses (D_e) values for the IR50 signal, with dot size representing $p0_{MAX}$. c. Probability density of $p0_{MAM}$ across all samples, and of $p0_{MAX}$ in d.

area and on the Bornrif platform showing higher values. The probability density distribution of $p0_{MAX}$ (Fig. 7d) is strongly skewed toward low values, even more so than $p0_{MAM}$ (Fig. 7c). A broad spatial pattern is visible: bMAX D_e values are highest at the northwestern tip of Ameland in the Borndiep and decrease along all potential transport pathways (Fig. 1). At the same time, $p0_{MAX}$ values tend to increase where bMAX D_e values decrease, indicating that a greater proportion of grains contribute to the maximum dose calculation. The large differences between the bMAM (Fig. 7a) and bMAX (Fig. 7b) equivalent doses indicate that the studied sediment samples contain grains with a high variety of absorbed doses, as is also visible from the abanico plots (Fig. 4 and Supplement S6 Figs. 5–62).

An overview of all bMAM, CAM, and bMAX values, including the number of grains per sample, $p0_{MAM}$, $p0_{MAX}$, and overdispersion, is

provided in the Supplement S3.

5. Discussion

5.1. Bleaching and mixing upon transport

Single-grain equivalent dose distributions (Fig. 4 and Section 4.1) show considerable overdispersion across the Ameland tidal inlet. We propose that this overdispersion arises from two principal processes:

1. Mixing of grains with different inherited doses, reflecting input from sediments of different ages.
2. Heterogeneous bleaching of grains reflecting differences in light exposure during (subaqueous) transport and deposition.

Both processes produce scattered D_e distributions, but combining the information obtained using signals of different bleachability may allow us to distinguish between the two processes. If scatter is dominated by mixing of sediments with different inherited doses, similar overdispersion in D_e distribution and also similar bMAX D_e is expected for signals of different bleachability for a sample. In contrast, heterogeneous bleaching yield signal-dependent discordances where grains may show low D_e in rapidly resetting IRSL50, yet retain higher D_e doses in slower pIRIR signals. Ideally, signals of different bleachability are compared for individual grains, but unfortunately our dataset did not yield sufficient signals per grain to do so (see Section 4.2).

Our equivalent dose models and associated bleaching metrics also lift a corner of the veil. For the IRSL50 D_e distribution, greatest overdispersion values (Fig. 6) and very high bMAX D_e (50–100 Gy) (Fig. 7b) near the northwestern tip of Ameland in the Borndiep coincide with locations where tidal currents erode into Pleistocene deposits (Fig. 2). In contrast, the low overdispersion and moderate CAM D_e (Fig. 6), but also bMAX D_e (Fig. 7b), values from samples derived from the ebb-tidal delta and the Bornrif suggest that the grains in these samples experienced higher bleaching opportunities prior to (re)deposition and/or little mixing with grains inheriting higher doses. This spatial pattern points to a gradual transition from samples containing grains with greater inherited doses to sediments that are progressively bleached along the dominant transport pathways.

The proportions of grains contributing to the bMAM and bMAX models for the IRSL50 signal reflect this line of reasoning. Low bMAM D_e values and small $p0_{MAM}$ (Fig. 7a and c) indicate that for most samples only a few grains with low dose contribute to the bMAM D_e estimate. In contrast, higher $p0_{MAM}$ offshore on the Bornrif suggest progressive bleaching during transport. The progressive decrease of bMAX offshore on the Bornrif, alongside increasing $p0_{MAX}$ values, suggests that transport and mixing with Holocene material lead to gradual dilution of old grains and incremental bleaching. This pattern implies that the Pleistocene eroded layers in the Bornrif act as a local source of grains with high doses, with light exposure during downstream transport reducing their dose.

The differences in remnant dose we observe for different feldspar signals (Fig. 5a-d) are consistent with their relative bleaching rates as documented in bleaching experiments at Texel (de Boer et al., 2024b) and in the Ameland Inlet (de Boer et al., 2024a, 2024b, in press). There we demonstrated that mineral-specific photo-ionization cross sections and wavelength-dependent light attenuation govern subaqueous bleaching efficiency. Tidal variations in suspended sediment concentration (SSC) further control bleaching conditions (de Boer et al., 2024a, 2024b, in review; Mauz et al., 2010). During ebb tide, elevated SSC causes strong light attenuation and longer bleaching durations, whereas clearer flood waters allow deeper light penetration and faster resetting (de Boer et al., 2024a, 2024b, in press).

Grain size also influences transport and bleaching opportunities: coarser grains tend to remain near the bed, while finer grains are more easily suspended and thus more likely to be exposed to light. Importantly, Pearson et al. (2021a) demonstrated via field measurements that sand in the 212–250 μm size range is easily suspended on Ameland ebb-tidal delta during spring tides and even small storms. Since this fraction also reflects the d50 of the Ameland inlet (Elias et al., 2022; Van Prooijen et al., 2020), it is a representative choice to investigate sediment transport routes for this system. We suggest that it would be highly interesting to investigate grain size dependency of both transport pathways and bleaching opportunities in future studies.

The observed variability in bleaching (Figs. 4–7) support the concept of "variable bleaching rules" proposed by (Mauz et al., 2010), who showed that bleaching efficiency in tidal settings cannot be tied to fixed sub-environments. SSC, water depth, and reworking frequency fluctuate strongly in space and time. Our Ameland data mirrors this complexity: grains record diverse bleaching and mixing histories that are a result of multiple transport events and inherited geological doses, where frequent resuspension and repeated light exposure gradually increase the degree of bleaching (Mauz et al., 2010; Pannozzo et al., 2023).

Full disentanglement of processes can only be done by comparing bleachability on grain level (Choi et al., 2024; Rhodes and Leathard, 2022). Our data unfortunately does not support this since we could not obtain enough grains with bright luminescence signals for all pIRIR signals (Section 4.3). For future research we advise to measure only one or two pIRIR signals on every grain if dealing with dim samples to increase signal intensity and thereby elevate grain acceptance rates, as this would enable comparison of bleachability between feldspar signals on the grain level (Choi et al., 2024). Nevertheless, application of a multitude of equivalent dose models did for the first time enable us to investigate spatial patterns in bleaching from sand-sized sediment from modern subtidal deposits.

5.2. Geological and morphodynamic controls on luminescence

As described in section 5.1 the spatial trends in equivalent dose (Figs. 4–7) and bleaching metrics (Figs. 6 and 7) across the Ameland inlet can be understood in the context of local geology (mixing) and modern morphodynamics (bleaching). As outlined in section 2.1 the Ameland tidal inlet forms a complex, constantly active sediment-sharing system with the North and Wadden Sea. The flood-dominant tidal asymmetry promotes net eastward sediment transport around the ebb-tidal delta (Elias et al., 2019). Wave forcing drives additional onshore and longshore transport, resulting in continuous reworking of nearshore deposits, which is also visible on the bathymetric overlay map in Fig. 3 and cross-section in Fig. 2: according to bathymetry-derived stratigraphic model of Pearson et al. (2022), most surface deposits along the transect through the Borndiep are very young (<25 years) and often reworked. This hydrodynamic regime translates into a sediment transport system characterized by strong temporal and spatial variability. According to modelling studies and bathymetry measurements, sediment is routed eastward from Terschelling toward Ameland via two dominant pathways (Fig. 1):

1. Suspension and export through the main ebb channel (Borndiep);
2. Wave- and tide-driven bypassing over the outer delta and Bornrif platform (Elias et al., 2019; Pearson et al., 2022).

The continuous clockwise rotation of the ebb-tidal delta (14°/year) (Fig. 1) causes progressive reworking of deposits, as can also be concluded from the bathymetric data (Fig. 3), while deep ebb channels erode into older substrates on their eastern flanks (Fig. 2). This process exposes Pleistocene deposits (Fig. 2, NUUR1 formation) along the channel margins, providing an immediate source of older material into the modern sediment transport system. Note that according the GeoTOP model cross-section (Fig. 2) this Urk Formation (NUUR1) from the Pleistocene has not been exposed in roughly 25 years. Bear in mind that the GeoTOP model is based on interpolations between a limited number of cores. Therefore, it is still possible that the Pleistocene material was

exposed here or elsewhere nearby, as corroborated by our luminescence dataset.

The luminescence data reflects these bleaching processes driven by hydrodynamics and mixing processes driven by introduction of older geological deposits. In areas where the substrate consists of well-reworked Holocene sands such as the Bornrif platform, overdispersion values are low and CAM estimates are consistent between samples located close to each other (Fig. 6). This highly likely indicates sediment populations dominated by repeated reworking within the upper active layer. In contrast, the northwestern tip of Ameland, where the Borndiep channel cuts into Pleistocene deposits (van Weerdenburg et al., 2021; Forzoni et al., 2018), exhibits higher overdispersion (Fig. 6) and larger differences between bMAM and bMAX (Fig. 7), indicating that only a small fraction of grains carries a luminescence dose from older deposits. Comparative dose rate determinations from the Wadden Sea (Madsen et al., 2010) would indicate that equivalent doses exceeding ~20 Gy likely reflect grains of at least Pleistocene age. Therefore, we interpret these grains to be eroded from the older NUUR1 deposits and not sourced from beach and/or shoreface nourishments, since these nourishment sands are of Holocene age (Fig. 3). Presence of non-bleached old grains is possible: de Boer et al. (2025 in review) quantitatively showed that the zone of sufficient bleaching duration for feldspar grains is limited to the upper few meters in the water column.

Future work should disentangle the mixing and bleaching forcings more explicitly by combining the defined luminescence-based bleaching metrics in this work (overdispersion, bMAM p0, bMAX p0 and dose models) with Lagrangian particle tracking models (van Westen et al., 2025) and connectivity analysis (Pearson et al., 2020). This combination of luminescence tracer data and Lagrangian modelling shows potential for checking whether the Eulerian morphodynamic models relied on to predict coastal evolution (e.g. Lesser et al., 2004) are getting "the right answers for the right reasons" (c.f. Kirchner, 2006; McDonnell et al., 2010).

5.3. Where did the nourished sand go?

Across the Ameland tidal inlet, nourished and native sands are indistinguishable in their luminescence signals measured in this work. Equivalent dose distributions (Fig. 4) are scattered and do not contain an identifiable group of grains that can be assigned to the nourishment. Likewise, overdispersion values (Fig. 6), and dose models and their metrics (Fig. 6–7) show spatial gradients yet no offset of grain populations separating nourished from native material. We propose that this outcome reflects two processes. First, the nourishment material was sourced from local Holocene deposits (the borrow area in Fig. 3), and therefore carried a luminescence fingerprint too similar to the native sediment. This situation is unlike that of Reimann et al. (2015), who successfully traced Pleistocene-derived nourishment material against Holocene beaches. Second, the dynamic inlet environment rapidly reworks and mixes deposited sand, erasing any small initial offset. Where spatial patterns in luminescence fingerprints are observed, they are better explained by mixing with older inherited grains and/or transport-related exposure histories (Section 5.2) than by the presence of a nourished component.

Luminescence tracing of this particular nourishment is not feasible with the feldspar signals and sampling density in our study. Distinction would require either a substantially larger initial dose contrast between nourished and native sediments, within grain comparison of bleachability (e.g., Choi et al., 2024) of all feldspar signals including TL, or targeting alternative signals such as quartz OSL that may amplify short-term exposure contrast because of higher signal bleachability (de Boer et al., 2025, in press). We suggest that tracking nourishment dispersal with luminescence may still be a viable strategy for this or other sites, depending on measurement strategies and local sediment characteristics.

5.4. Relevant timescales

Luminescence tracing studies may capture sediment mobility on different timescales, ranging from individual storm events to centuries or even millennia. The relevant time scale will depend on a wide range of factors including the difference in luminescence fingerprint between source materials, the dynamics of the system, the light exposure during transport, and the light sensitivity of the luminescence signals used. Reimann et al. (2015) showed that luminescence profiling can identify nourishment sand transported within months-years. In the present study we could not differentiate between nourishment sand and native grains, but identified transport pathways that likely reflect short-term dynamics, on the order of months to years, and differences in source material reflecting inherited (geological) conditions.

6. Conclusions

This study demonstrates for the first time that single-grain feldspar luminescence signals capture spatial bleaching and mixing dynamics of modern coastal sand sized sediments in a tidal inlet. Spatial trends in equivalent dose distributions, equivalent dose models, and dose model metrics reflect a combination of (1) heterogeneous bleaching during transport and (2) mixing with sediments that inherited Pleistocene luminescence doses. The highest equivalent doses occur near the northwestern tip of Ameland in the Borndiep channel where local erosion supplies older (Pleistocene) material into the mix. Along all potential sediment pathways, these equivalent doses become progressively lower because of gradual bleaching during transport. In areas where the substrate consists of well-reworked Holocene sands such as the ebb-tidal delta and the Bornrif platform, lower equivalent doses highly likely indicate that sediment populations are dominated by repeated reworking within the upper active layer. Nourished and native sediments were found to show indistinguishable luminescence characteristics for our dataset due to their shared Holocene origin, preventing the use of the luminescence methods tested here to trace nourishment sand. Together, these results demonstrate that we can interpret modern coastal spatial bleaching patterns based on morphodynamics and geology and that tracking nourishment dispersal with luminescence can be a viable strategy but its success highly depends on measurement strategies and local sediment characteristics. For future work, we suggest it may be beneficial to measure fewer pIRIR signals to boost signal intensity and elevate acceptance rates. This would allow inferences of light-exposure history at single-grain level by comparison of equivalent dose of signals of different bleachability.

CRediT authorship contribution statement

Anna Maartje de Boer: Writing – review & editing, Writing – original draft, Visualization, Validation, Software, Project administration, Methodology, Investigation, Formal analysis, Data curation, Conceptualization. **Stuart Pearson:** Writing – review & editing, Writing – original draft, Visualization, Software, Resources, Funding acquisition, Conceptualization. **Ad van der Spek:** Writing – review & editing, Writing – original draft, Visualization, Software, Resources. **Bram van Prooijen:** Writing – review & editing, Supervision, Funding acquisition, Conceptualization. **Jakob Wallinga:** Writing – review & editing, Validation, Supervision, Resources, Project administration, Methodology, Investigation, Funding acquisition, Formal analysis, Conceptualization.

Funding sources

This work is part of TRAILS (TRacking Ameland Inlet living Lab Sediment) and was funded by the Dutch research council (NWO), project 17600. SP is funded by project 21026 Revealing Hidden Networks of Coastal Sediment Pathways via Laboratory & Numerical Experiments, also supported by the Dutch Research Council (NWO).

Declaration of generative AI and AI-assisted technologies in the manuscript preparation process.

During the preparation of this work the author(s) used ChatGPT (Open AI) in order to provide language support, and to enhance the clarity of the text. After using this tool/service, the author(s) reviewed and edited the content as needed and take(s) full responsibility for the content of the published article.

Declaration of competing interest

The authors declare that they have no known competing financial interests or personal relationships that could have appeared to influence the work reported in this paper.

Acknowledgements

We thank Rob Witbaard (NIOZ) for providing samples collected with RV Pelagia (NCL-1121), and the SEAWAD project for sharing their 2017 samples (NCL-1321). We are grateful to the crew of RV Navicula for supporting our sampling campaigns (NCL-1222 and NCL-1821). Special thanks to Tjitske Kooistra for her unwavering assistance with boxcore sampling during the cruises, and to Alice Versendaal and Erna van den Hengel-Voskuilen for their help in the NCL laboratory.

Appendix A. Supplementary data

Supplementary data to this article can be found online at https://doi.org/10.1016/j.margeo.2026.107749.

Data availability

All raw data, analysis code, and output data supporting this study is published on Wageningen University & Research data share called YODA under DOI https://doi.org/10.17887/WUR01-LWMSLD.

References

Ahmed, M., Sato, S., Tajima, Y., 2014. Quantitative estimation of longshore sediment transport based on thermoluminescence: two case studies around Tenryu and Nile River Mouths. J. Coast. Res. 30 (3), 537–547.

Black, K.S., Athey, S., Wilson, P., Evans, D., 2007. The use of particle tracking in sediment transport studies: a review. Geol. Soc. Lond. Spec. Publ. 274 (1), 73–91.

Brand, E., Ramaekers, G., Lodder, Q., 2022. Dutch experience with sand nourishments for dynamic coastline conservation–an operational overview. Ocean Coast. Manag. 217, 106008.

Brand, E., Lodder, Q., Quataert, E., Slinger, J., 2025. Sustainable coastline management-the cumulative effects of 30 years of nourishments in the Netherlands. Ocean Coast. Manag. 270, 107895.

Brill, D., Reimann, T., Wallinga, J., May, S., Engel, M., Riedesel, S., Brückner, H., 2018. Testing the accuracy of feldspar single grains to date late Holocene cyclone and tsunami deposits. Quat. Geochronol. 48, 91–103. https://doi.org/10.1016/j.quageo.2018.09.001.

Cheng, T., Zhang, D., Zhao, H., Yang, S., Li, B., 2022. Bleachability of pIRIR signal from single-grain K-feldspar. Quat. Geochronol. 71, 101321. https://doi.org/10.1016/j.quageo.2022.101321.

Choi, J., Chamberlain, E., Wallinga, J., 2024. Variance in pIRIR Signal Bleaching for Single Grains of Feldspar. Elsevier.

Clemens, K.E., Komar, P.D., 1988. Tracers of sand movement on the Oregon coast. In *Coastal Engineering 1988* (pp. 1338-1351).

Crickmore, M., Lean, G., 1962. The measurement of sand transport by means of radioactive tracers. Proceedi. Royal Soc. London. Series Mathemat. Phys. Sci. 266 (1326), 402–421.

Cunningham, A.C., Wallinga, J., 2012. Realizing the potential of fluvial archives using robust OSL chronologies. Quat. Geochronol. 12, 98–106.

Cunningham, A.C., Wallinga, J., Hobo, N., Versendaal, A.J., Makaske, B., Middelkoop, H., 2015. Re-Evaluating Luminescence Burial Doses and Bleaching of Fluvial Deposits Using Bayesian Computational Statistics.

de Boer, A., Kook, M., Wallinga, J., 2024a. Testing the performance of an EMCCD camera in measuring single-grain feldspar (thermo) luminescence in comparison to a laser-based single-grain system. Radiat. Meas. 175, 107168. https://doi.org/10.1016/j.radmeas.2024.107168.

de Boer, A., Seebregts, M., Wallinga, J., Chamberlain, E., 2024b. A one-day experiment quantifying subaqueous bleaching of K-feldspar luminescence signals in the Wadden Sea, the Netherlands. Neth. J. Geosci. 103, e22.

Deeben, J., Hiddink, H., Huisman, D., Müller, A., Schokker, J., Wallinga, J., 2010. Middle Palaeolithic artefact migration due to periglacial processes; a geological investigation into near-surface occurrence of Palaeolithic artefacts (Limburg-Eastern Brabant coversand region, the Netherlands). Neth. J. Geosci. 89 (1), 35–50.

Dietze, M., Kreutzer, S., Burow, C., Fuchs, M.C., Fischer, M., Schmidt, C., 2016. The abanico plot: visualising chronometric data with individual standard errors. Quat. Geochronol. 31, 12–18.

Donatelli, C., Duran-Matute, M., Gräwe, U., Gerkema, T., 2022. Residual circulation and freshwater retention within an event-driven system of intertidal basins. J. Sea Res. 186, 102242.

Duller, G.A., 2008. Single-grain optical dating of Quaternary sediments: why aliquot size matters in luminescence dating. Boreas 37 (4), 589–612.

Duran-Matute, M., Gerkema, T., De Boer, G., Nauw, J., Gräwe, U., 2014. Residual circulation and freshwater transport in the Dutch Wadden Sea: a numerical modelling study. Ocean Sci. 10 (4), 611–632.

Eisma, D., Berger, G., Wei-Yue, C., Jian, S., 1989. Pb-210 as a tracer for sediment transport and deposition in the Dutch-German Waddensea. In: Coastal Lowlands: Geology and Geotechnology. Springer, pp. 237–253.

Elias, E., Van der Spek, A., Wang, Z.B., De Ronde, J., 2012. Morphodynamic development and sediment budget of the Dutch Wadden Sea over the last century. Neth. J. Geosci. 91 (3), 293–310.

Elias, E., Van der Spek, A., Pearson, S., Cleveringa, J., 2019. Understanding sediment bypassing processes through analysis of high-frequency observations of Ameland Inlet, the Netherlands. Mar. Geol. 415, 105956.

Elias, E., Pearson, S., van der Spek, A., Pluis, S., 2022. Understanding meso-scale processes at a mixed-energy tidal inlet: Ameland Inlet, the Netherlands–implications for coastal maintenance. Ocean Coast. Manag. 222, 106125.

Forzoni, A.H., Marc, Vermaas, Tommer, 2018. Geologie en morfodynamiek getijdengeulen, casus Borndiep, Zuidwest. Ameland.

Galbraith, R., Roberts, R., Laslett, G., Yoshida, H., Olley, J., 1999. Optical dating of single and multiple grains of quartz from Jinmium rock shelter, northern Australia: part I, experimental design and statistical models. Archaeometry 41 (2), 339–364.

Gallaway, E., Trenhaile, A.S., Cioppa, M.T., Hatfield, R.G., 2012. Magnetic mineral transport and sorting in the swash-zone: northern Lake Erie, Canada. Sedimentology 59 (6), 1718–1734.

Giffin, D., Corbett, D.R., 2003. Evaluation of sediment dynamics in coastal systems via short-lived radioisotopes. J. Mar. Syst. 42 (3–4), 83–96.

Gray, H., Jain, M., Sawakuchi, A., Mahan, S., Tucker, G., 2019. Luminescence as a sediment tracer and provenance tool. Rev. Geophys. 57 (3), 987–1017. https://doi.org/10.1029/2019RG000646.

Guyez, A., Bonnet, S., Reimann, T., Carretier, S., Wallinga, J., 2022. Illuminating past river incision, sediment source and pathways using luminescence signals of individual feldspar grains (Rangitikei River, New Zealand). Earth Surf. Process. Landf. https://doi.org/10.1002/esp.5357.

Guyez, A., Bonnet, S., Reimann, T., Carretier, S., Wallinga, J., 2023. A Novel Approach to Quantify Sediment transfer and Storage in Rivers—Testing Feldspar Single-Grain pIRIR Analysis and Numerical Simulations. J. Geophys. Res.: Earth Surf. 128 (2), e2022JF006727. https://doi.org/10.1029/2022JF006727.

Huntley, D.J., Godfrey-Smith, D.I., Thewalt, M.L., 1985. Optical dating of sediments. Nature 313 (5998), 105–107.

Kars, R., Reimann, T., Wallinga, J., 2014. Are feldspar SAR protocols appropriate for post-IR IRSL dating? Quat. Geochronol. 22, 126–136.

Kirchner, J.W., 2006. Getting the right answers for the right reasons: linking measurements, analyses, and models to advance the science of hydrology. Water Resour. Res. 42 (3).

Kook, M., Lapp, T., Murray, A., Thomsen, K., Jain, M., 2015. A luminescence imaging system for the routine measurement of single-grain OSL dose distributions. Radiat. Meas. 81, 171–177. https://doi.org/10.1016/j.radmeas.2015.02.010.

Kraus, N.C., Isobe, M., Igarashi, H., Sasaki, T.O., Horikawa, K., 1982. Field experiments on longshore sand transport in the surf zone. In: Coastal Engineering, 1982, pp. 969–988.

Kreutzer, M.S., Developers, C.P., 2025. Package 'Luminescence'.

Lesser, G.R., Roelvink, J.v., van Kester, J.T.M., Stelling, G., 2004. Development and validation of a three-dimensional morphological model. Coast. Eng. 51 (8–9), 883–915.

Madsen, A.T., Murray, A.S., Andersen, T.J., Pejrup, M., 2010. Luminescence dating of Holocene sedimentary deposits on Rømø, a barrier island in the Wadden Sea, Denmark. The Holocene 20 (8), 1247–1256.

Mauz, B., Baeteman, C., Bungenstock, F., Plater, A., 2010. Optical dating of tidal sediments: potentials and limits inferred from the North Sea coast. Quat. Geochronol. 5 (6), 667–678.

McDonnell, J., McGuire, K., Aggarwal, P., Beven, K., Biondi, D., Destouni, G., Dunn, S., James, A., Kirchner, J., Kraft, P., 2010. How old is streamwater? Open questions in catchment transit time conceptualization, modelling and analysis. Hydrol. Process. 24 (12), 1745–1754.

Miller, M.C., Komar, P.D., 1979. Measurements of sand spreading rates under near-bottom wave orbital motions. J. Geol. 87 (6), 593–608.

Murray, S.P., 1967. Control of grain dispersion by particle size and wave state. J. Geol. 75 (5), 612–634.

Oliveira, S., Moura, D., Horta, J., Nascimento, A., Gomes, A., Veiga-Pires, C., 2017. The morphosedimentary behaviour of a headland–beach system: Quantifying sediment transport using fluorescent tracers. Mar. Geol. 388, 62–73.

Olley, J.M., De Deckker, P., Roberts, R.G., Fifield, L.K., Yoshida, H., Hancock, G., 2004. Optical dating of deep-sea sediments using single grains of quartz: a comparison with radiocarbon. Sediment. Geol. 169 (3–4), 175–189.

Pannozzo, N., Smedley, R., Plater, A., Carnacina, I., Leonardi, N., 2023. Novel luminescence diagnosis of storm deposition across intertidal environments. Sci. Total Environ. 867, 161461.
Pannozzo, N., Pearson, S., Meijer, M., de Boer, A.-M., de Wilde, T., Elias, E., Kooistra, T., Wallinga, J., Van Prooijen, B., 2025. Tracing sand transport pathways using a Lagrangian sediment tracking model.
Pearson, S., 2022. Sediment Pathways on Ebb-Tidal Deltas: New Tools and Techniques for Analysis. Delft University of Technology.
Pearson, S., van Prooijen, B.C., Elias, E.P., Vitousek, S., Wang, Z.B., 2020. Sediment connectivity: a framework for analyzing coastal sediment transport pathways. J. Geophys. Res.: Earth Surf. 125 (10), e2020JF005595.
Pearson, S., van Prooijen, B., Poleykett, J., Wright, M., Black, K., Wang, Z.B., 2021a. Tracking fluorescent and ferrimagnetic sediment tracers on an energetic ebb-tidal delta to monitor grain size-selective dispersal. Ocean Coast. Manag. 212, 105835.
Pearson, S., Verney, R., van Prooijen, B., Tran, D., Hendriks, E., Jacquet, M., Wang, Z., 2021b. Characterizing the composition of sand and mud suspensions in coastal and estuarine environments using combined optical and acoustic measurements. J. Geophys. Res. Oceans 126 (7), e2021JC017354.
Pearson, S., Elias, E., van Prooijen, B., van der Vegt, H., van der Spek, A.J., Wang, Z., 2022. A novel approach to mapping ebb-tidal delta morphodynamics and stratigraphy. Geomorphology 405, 108185.
Pierik, H.J., Leuven, J.R., Busschers, F.S., Hijma, M.P., Kleinhans, M.G., 2023. Depth-limiting resistant layers restrict dimensions and positions of estuarine channels and bars. Depositional Rec. 9 (2), 213–232.
Reimann, T., Notenboom, P., De Schipper, M., Wallinga, J., 2015. Testing for sufficient signal resetting during sediment transport using a polymineral multiple-signal luminescence approach. Quat. Geochronol. 25, 26–36. https://doi.org/10.1016/j.quageo.2014.09.002.
Rhodes, E., 2011. Optically stimulated luminescence dating of sediments over the past 200,000 years. Annu. Rev. Earth Planet. Sci. 39, 461–488.
Rhodes, E.J., Leathard, J.A., 2022. MET-IRSL used to track pre-depositional sediment transport history. Quat. Geochronol. 70, 101294. https://doi.org/10.1016/j.quageo.2022.101294.
Ridderinkhof, W., Hoekstra, P., Van der Vegt, M., De Swart, H., 2016. Cyclic behavior of sandy shoals on the ebb-tidal deltas of the Wadden Sea. Cont. Shelf Res. 115, 14–26.
Rodnight, H., Duller, G., Wintle, A., Tooth, S., 2006. Assessing the reproducibility and accuracy of optical dating of fluvial deposits. Quat. Geochronol. 1 (2), 109–120.
Romão, S., Cascalho, J., Ferreira, C.C., Font, E., Taborda, R., Silva, P.A., Duarte, J.F., Staudt, F., 2024. Testing magnetic tracers as indicators of sediment transport in a wave flume experiment. Sedimentology 71 (5), 1498–1514.
Straaten, L.M.J.U., 1954. Composition and Structure of Recent Marine Sediments in the Netherlands.
Thomsen, K.J., Murray, A.S., Jain, M., Bøtter-Jensen, L., 2008. Laboratory fading rates of various luminescence signals from feldspar-rich sediment extracts. Radiat. Meas. 43 (9–10), 1474–1486.
TNO-GDN, 2025. DINOloket, Data and information on the Dutch Subsurface. https://www.dinoloket.nl/en/subsurface-models/map.
van der Spek, A.J.F., 2018. The development of the tidal basins in the Dutch Wadden Sea until 2100: the impact of accelerated sea-level rise and subsidence on their sediment budget – a synthesis. Neth. J. Geosci. 97 (3), 71–78. https://doi.org/10.1017/njg.2018.10.
van der Spek, A., Forzoni, A., Vermaas, T., 2022. Holocene deposits at the lower shoreface and inner shelf of the Dutch coast. Ocean Coast. Manag. 224, 106203.
van Heteren, S., van der Spek, A., 2003. Long-Term Evolution of a Small Estuary: The Lauwerszee (Northern Netherlands), Report NITG 03–108-a. Netherlands Institute of Applied Geoscience TNO-National Geological Survey, Utrecht.
van Onselen, E., 2020. Moeilijk erodeerbare lagen in de Waddenzee en Westerschelde, kartering en effect op morfologische ontwikkeling van geulen.
Van Prooijen, B.C., Tissier, M.F., De Wit, F.P., Pearson, S.G., Brakenhoff, L.B., Van Maarseveen, M.C., Van Der Vegt, M., Mol, J.-W., Kok, F., Holzhauer, H., 2020. Measurements of hydrodynamics, sediment, morphology and benthos on Ameland ebb-tidal delta and lower shoreface. Earth Syst. Sci. Data 12 (4), 2775–2786.
Van Straaten, L., 1964. De bodem der Waddenzee. In: Het waddenboek, pp. 75–151.
van Weerdenburg, R., Pearson, S., van Prooijen, B., Laan, S., Elias, E., Tonnon, P.K., Wang, Z.B., 2021. Field measurements and numerical modelling of wind-driven exchange flows in a tidal inlet system in the Dutch Wadden Sea. Ocean Coast. Manag. 215, 105941.
van Westen, B., de Schipper, M.A., Pearson, S.G., Luijendijk, A.P., 2025. Lagrangian modelling reveals sediment pathways at evolving coasts. Sci. Rep. 15 (1), 8793.
Veenstra, H.J., Winkelmolen, A.M., 1976. Size, Shape and Density Sorting around Two Barrier Islands along the North Coast of Holland.
Vermaas, T., 2018. Geologie, bestorting en strandvallen bij Ameland zuidwest - eindrapportage 2019.
Wang, Z.B., Elias, E.P.L., van der Spek, A.J.F., Lodder, Q.J., 2018. Sediment budget and morphological development of the Dutch Wadden Sea: impact of accelerated sea-level rise and subsidence until 2100. Neth. J. Geosci. 97 (3), 183–214. https://doi.org/10.1017/njg.2018.8.